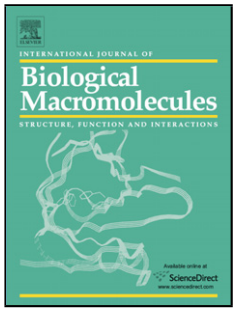

Title: Structural dynamics of a single-chain Fv antibody against (4-hydroxy-3-nitrophenyl)acetyl

Author: Yusui Sato Yusuke Tanaka Satomi Inaba Hiroshi Sekiguchi Takahiro Maruno Yuji C. Sasaki Harumi Fukada Yuji Kobayashi Takachika Azuma Masayuki Oda

PII: S0141-8130(16)30486-X
DOI: http://dx.doi.org/doi:10.1016/j.ijbiomac.2016.05.074
Reference: BIOMAC 6135

To appear in: *International Journal of Biological Macromolecules*

Received date: 25-1-2016
Revised date: 18-5-2016
Accepted date: 20-5-2016

Please cite this article as: Yusui Sato, Yusuke Tanaka, Satomi Inaba, Hiroshi Sekiguchi, Takahiro Maruno, Yuji C.Sasaki, Harumi Fukada, Yuji Kobayashi, Takachika Azuma, Masayuki Oda, Structural dynamics of a single-chain Fv antibody against (4-hydroxy-3-nitrophenyl)acetyl, International Journal of Biological Macromolecules http://dx.doi.org/10.1016/j.ijbiomac.2016.05.074

Structural dynamics of a single-chain Fv antibody against (4-hydroxy-3-nitrophenyl)acetyl

Yusui Sato[1,a], Yusuke Tanaka[1,a], Satomi Inaba[1], Hiroshi Sekiguchi[2], Takahiro Maruno[3], Yuji C. Sasaki[4], Harumi Fukada[5], Yuji Kobayashi[3], Takachika Azuma[6], Masayuki Oda[1,*]

[1] Graduate School of Life and Environmental Sciences, Kyoto Prefectural University, 1-5 Hangi-cho, Shimogamo, Sakyo-ku, Kyoto, Kyoto 606-8522, Japan,

[2] Japan Synchrotron Radiation Research Institute, 1-1-1 Kouto, Sayo, Hyogo 679–5198, Japan,

[3] Graduate School of Engineering, Osaka University, 2-1 Yamadaoka, Suita, Osaka 565-0871, Japan,

[4] Graduate School of Frontier Sciences, The University of Tokyo, Kashiwanoha, Kashiwa, Chiba 277–8561, Japan,

[5] Graduate School of Life and Environmental Sciences, Osaka Prefecture University, 1-1 Gakuen-cho, Naka-ku, Sakai, Osaka 599-8531, Japan,

[6] Research Institute for Biological Sciences (RIBS), Tokyo University of Science, 2669 Yamazaki, Noda, Chiba 278-0022, Japan.

[a] These authors contributed equally to the work.

[*] To whom correspondence should be addressed.

Telephone: +81-75-703-5673

Fax: +81-75-703-5673

E-mail: oda@kpu.ac.jp

Abstract

Protein structure dynamics are critical for understanding structure-function relationships. An antibody can recognize its antigen, and can evolve toward the immunogen to increase binding strength, in a process referred to as affinity maturation. In this study, a single-chain Fv (scFv) antibody against (4-hydroxy-3-nitrophenyl)acetyl, derived from affinity matured type, C6, was designed to comprise the variable regions of light and heavy chains connected by a $(GGGGS)_3$ linker peptide. This scFv was expressed in *Escherichia coli* in the insoluble fraction, solubilized in the presence of urea, and refolded by stepwise dialysis. The correctly refolded scFv was purified, and its structural, physical, and functional properties were analyzed using analytical ultracentrifugation, circular dichroism spectrometry, differential scanning calorimetry, and surface plasmon resonance biosensor. Thermal stability of C6 scFv increased greatly upon antigen binding, due to favorable enthalpic contributions. Antigen binding kinetics were comparable to those of the intact C6 antibody. Structural dynamics were analyzed using the diffracted X-ray tracking method, showing that fluctuations were suppressed upon antigen binding. The antigen binding energy determined from the angular diffusion coefficients was in good agreement with that calculated from the kinetics analysis, indicating that the fluctuations detected at single-molecule level are well reflected by antigen binding events.

Keywords

antigen binding; single-molecule analysis; thermal stability

Introduction

Antibodies are capable of recognizing various types of antigens by antigen-combining sites, constructed mainly from amino acid residues in complementarity determining regions (CDRs). Primary antibodies produced at an early stage of immunization have low affinity toward the immunized antigen, while those secreted at a later stage have higher affinity. This observation is referred to as affinity maturation [1] and has been shown to be induced by somatic hypermutation [2,3]. Structural and functional analyses of antibodies on the pathway of affinity maturation can elucidate the molecular mechanism of protein recognition. Such analyses can also inform rational protein design, for example, by suggesting ways to increase the affinity and specificity of antibodies [4-6]. By analyzing many kinds of monoclonal antibodies during affinity maturation, their respective antigen recognition mechanisms can be investigated. The molecular insights obtained by studying *in vivo* evolution can be applied for rational design. One of the most important and challenging problems in this process should be to elucidate the structural dynamics induced upon antigen binding. Although great numbers of protein structures have been determined at atomic resolution using X-ray crystallography and NMR, most of these are static models representing only the most stable structure or the averaged structures. The conformational changes induced in antibodies upon antigen binding, together with the conformational selection processes present in the conformational ensembles of antibodies and/or antigens, are critical for a deeper understanding the structure-function relationship of antibodies [7-9].

In this study, we produced a single-chain Fv (scFv) antibody against (4-hydroxy-3-nitrophenyl)acetyl (NP), and analyzed its structural, physical, and functional properties. The advantages of generating scFv antibodies are as follows. First, tertiary structure and structural dynamics can be analyzed using NMR, because of the small size of scFv molecules relative to Fab and intact antibodies, while retaining

antigen binding ability [10,11]. Second, peptides or proteins could be appended to the N- and/or C-terminus of the scFv, when expressed in *Escherichia coli*. Third, the specific site of an scFv can be changed by site-directed mutagenesis, and its effects on structure and function can be analyzed. In the case of anti-NP antibodies, many monoclonal antibodies have been produced, and their affinity maturation process has been analyzed [12-14]. We can investigate the effects on structure and function of residues appearing in known monoclonal antibodies, but cannot assess the effects of residues or its combination unchanged in the antibodies. It is difficult to confirm whether antibodies different from those obtained as monoclonal antibodies are in fact generated but selected during the maturation process or not being generated. In the case of anti-NP antibodies, Azuma's group have shown that there are two key residues, the 33rd and 95th in the heavy chain, for affinity maturation [13,15]. Antibodies with Trp33 and Tyr95 appear at the early stage of immunization, and those with Leu33 and Tyr95 appear at the next stage, resulting in a ~10-fold increase in antigen binding affinity. At the later stages through another strategy that raises affinity ~100-fold, antibodies containing Trp33 and Gly95 appear. It will be interesting to understand the role of these two residues in the structural dynamics of the antibody and in the antigen recognition. As the first step, we expressed and purified an scFv derived from C6, an affinity matured antibody possessing Trp33 and Gly95 in the heavy chain. In this study, the diffracted X-ray tracking (DXT) method was applied to analyze the structural dynamics of the scFv [16-20]. Using an N-terminal His-tag, the scFv was immobilized on a Ni-NTA (nitrilotriacetic acid) substrate for the DXT measurement. Using this system, the scFv molecules can be arranged homogeneously for antigen binding with little steric hindrance. The DXT experiments could detect the structural dynamics of C6 scFv and its change upon the antigen binding at single-molecule level.

Materials and Methods

Expression and purification of scFv

Genes encoding the anti-NP scFv (-VL-$(G_4S)_3$ linker-VH-) were amplified by PCR using the template encoding VL and VH domains with following primers: VL-BamHI-sense: 5'-GAAAAGCGGATCCGCCCAGGCTGTTGTGACTC-3', VL-GS-antisense: 5'-ACCAGAGCCGCCGCCGCCGCTACCACCACCACCCTGGCCTAGGACAGTC-3', VH-GS-sense: 5'-AGCGGCGGCGGCGGCTCTGGTGGTGGTGGATCACAGGTCCAACTGCAG-3', VH-EcoRI-antisense: 5'-AAAAGAATTCTCATCATGAGGAGACTGTGAGAG-3'. The amplified gene fragment was inserted into plasmid pET-32TH slightly modified from pET-32a(+). The vector was transformed into *E. coli* BL21 (DE3) codon plus. The transformed cells were cultured in LB medium at 37°C. When the culture reached an A_{600} of about 0.6, isopropyl-β-D-thiogalactopyranoside (IPTG) was added to a final concentration of 0.1 mM. Cells were cultured for a further 12 h at 22°C. The harvested cells were suspended in 50 mM Tris-HCl (pH 9.0) buffer containing 150 mM NaCl, 1 mM EDTA, 1 mM DTT, and 0.5% Triton X-100, and lysed by sonication. The insoluble fraction was collected by centrifugation and resuspended in washing buffer, 50 mM Tris-HCl (pH 9.0) containing 150 mM NaCl, 1 mM EDTA, and 0.5% Triton X-100. This washing process was performed three times, and then, the sample was washed a further three times using washing buffer without Triton X-100 to remove the surfactant. Finally, the pellet was solubilized in solubilization buffer, 50 mM Tris-HCl (pH 9.0) containing 8 M urea, 150 mM NaCl, 1 mM EDTA, and 10 mM DTT. The solubilized scFv was refolded by stepwise dialysis. The urea concentration was decreased stepwise from 8 M to 0 M, via 4, 2, 1 M. As additives, 1 mM glutathione (oxidized form) and 0.4 M L-arginine were added at the 1 M urea step. Following dialysis, the solution was centrifuged to remove minor precipitation. In order to remove the thioredoxin-tag at the

N terminus of scFv, thrombin (Mochida Pharmaceutical Co., Ltd.) was added, and the solution was incubated overnight at 4ºC. Finally, the scFv was purified using an antigen column, in which NP conjugated to BSA was immobilized on the resin (NHS-activated sepharose 4; GE Healthcare). Captured scFv on the column was eluted with 10 mM Gly-HCl (pH 2.7) and neutralized immediately with 2 M Tris-HCl (pH 9.0). The concentration of scFv was calculated with molar absorption coefficient of 5.64×10^3 M^{-1} cm^{-1} at 280 nm. The plasmid encoding the N54M mutant scFv was generated by site-directed mutagenesis, and the protein was expressed and purified in the same manner.

Antigen preparation

NP-coupled ε-aminocaproic acid (NP-Cap), NP-coupled bovine serum albumin (BSA) at a molar ratio of 8.2:1 ($NP_{8.2}$-BSA), and (4-hydroxy-3,5-dinitrophenyl)acetyl (NNP) -coupled BSA at a molar ratio of 6.4:1 ($NNP_{6.4}$-BSA) were prepared as described previously [21]. The concentrations of NP and NNP were determined using molar absorption coefficients of 4.23×10^3 M^{-1} cm^{-1} at 430 nm and 7.12×10^3 M^{-1} cm^{-1} at 445 nm, respectively [22].

Analytical ultracentrifugation experiments

Analytical ultracentrifugation sedimentation velocity (AUC-SV) experiments were performed using a Beckman Optima XL-A analytical ultracentrifuge equipped with the 4-hole An60 Ti rotor at 20°C using double-sector centerpieces with the quartz windows. The concentration of scFv was 20 μM (A_{280} = 1.2) in PBS and the speed of rotation was 60,000 rpm. A radial step size of 0.003 cm was used for scanning which was carried out for 2 min in continuous scan mode and data was collected using absorbance optics at 285 nm. The distribution of sedimentation coefficient was analyzed

using c(s) method of Program SEDFIT [23]. The position of the meniscus and the cell bottom were floated during the fitting.

CD experiments

Far UV CD spectra were measured in 40 mM potassium phosphate buffer (pH 7.3) at 20ºC on a Jasco J-820 spectropolarimeter. The scFv concentration was 0.02 mg/ml. CD spectra were obtained under the following condition: optical path length of 1 cm, scan rate of 20 nm/min, response time of 1 sec, and bandwidth of 1 nm.

DSC experiments

Thermal stability of scFv was analyzed using Nano-DSC II calorimeter (TA instruments). Solution of scFv at 0.4 mg/ml in 40 mM potassium phosphate buffer (pH 7.3) was heated from 20 to 80ºC at a scan rate of 1.0ºC /min. Collected data were analyzed on origin software and midpoints of thermal denaturation (T_d), heat capacity change (ΔC_p) at T_d, and calorimetric enthalpy change (ΔH_{cal}) were calculated by fitting analysis [24]. The van't Hoff enthalpy change (ΔH_{vH}) was estimated from following equation,

$$\Delta H_{vH}(T_d) = 4RT_d^2 \frac{C_p(T_d)}{\Delta H_{cal}(T_d)} \qquad (1)$$

where C_p is the molar excess heat capacity, and R is the universal gas constant. The Gibbs free energy of unfolding as a function of temperature, $\Delta G_m(T)$, could be calculated from the following equation,

$$\Delta G_m(T) = \Delta H_{cal}(T_d)\left(1-\frac{T}{T_d}\right) - \Delta C_p T \ln \frac{T}{T_d} - \Delta C_p(T_d - T) \qquad (2)$$

SPR experiments

Antigen-antibody interactions were analyzed using SPR biosensor (Biacore T200, GE Healthcare). Antigens, $NP_{8.2}$-BSA and $NNP_{6.4}$-BSA were immobilized on the

dextran surface of a CM5 sensorchip (GE Healthcare) with amine coupling method. ScFv was diluted at eleven concentrations (0.781, 1.56, 3.13, 6.25, 12.5, 25.0, 50.0, 100, 200, 400, and 800 nM) in PBS containing 0.005% Tween 20 (running buffer) and the association of each solution was recorded at rate of 20 μl/min for 3 min. The dissociation of the complexes was measured by injecting running buffer alone for 3 min, followed by injecting of 3 M Gdn-HCl containing 1 M acetate for 45 s as regeneration. The experiments were performed at 25ºC and collected data were analyzed using the BIAevaluation 3.1 software. The sensorgrams were first examined by adjusting for background changes reflected in the bulk refractive index, using sensorgrams of interactions between C6 scFv and negative control dextran surface on the chip. Obtained curves were fitted to a 1:1 binding model using global fitting method to determine the kinetic rate constants, association rate constant (k_{on}) and dissociation rate constant (k_{off}). The association constant (K_a) was calculated from the two rate constants: $K_a = k_{on}/ k_{off}$.

DXT experiments

The target protein was labeled with a gold-nanocrystal which was used as a motion tracer. The angular displacement of the nanocrystal was analyzed about two rotational axes, tilting (θ) and twisting (χ) directions. Polyimide films (50 μm thick, Kapton, Du Pont-Toray, Tokyo, Japan) were coated with elemental chromium (4 nm) and gold (10 nm) by vapor deposition, and used as a substrate. The substrate was soaked overnight at 4°C in 1.6 mM 3,3'-dithiobis[N-(5-amino-5-carboxypentyl)propionamide-N',N'-diacetic acid] (Dithiobis (C_2-NTA), Dojindo Laboratories) dissolved in ethanol. The modified substrate was washed with ethanol, and then soaked for 4 h at 4°C in 100 mM $NiSO_4$ dissolved in 50 mM MOPS (pH 7.0) to generate Ni^{2+}-chelates. His-tagged protein solution was loaded on the Ni^{2+}-treated substrate for 7 h at 4°C. Gold-nanocrystals were

obtained by vacuum evaporation on a NaCl or KCl (100) surface [25] and dissolved with detergent, n-decyl-β-D-maltoside (Dojindo Laboratories), in 50 mM MOPS (pH 7.0). The gold-nanocrystal solution was applied to the protein immobilized on the substrate, and incubated for 7 h at 4°C. This was followed by washing and filling the upper space of substrate in the experimental chamber (~7 μl) with the HBS buffer solution of 10 mM HEPES (pH 7.3) and 140 mM NaCl in the absence or presence of 0.3 mM NP-Cap. DXT measurements were performed using synchrotron radiation at SPring-8 (Japan), on high-flux beamline BL40XU. Photon flux at the sample position is estimated to be ~10^{15} photon/sec/mm^2 in an energy range from 14.0 - 16.5 keV. The incident X-ray beam was about 50 μm in diameter. Diffraction images were collected with an X-ray image intensifier (Hamamatsu Photonics, V5445P) and a CMOS camera (SA1.1, Photron, Japan). To trace diffracted spots, Particle Track and Analysis: PTA (Copyright (2010) Yoshiyuki Arai) was used and trajectories were analyzed using custom software written for *IGOR Pro* (Wavemetrics, Lake Oswego, OR).

Results

An scFv of anti-NP monoclonal antibody, C6, was designed for this study. VL and VH regions were connected by a linker region comprising three repeats of the peptide, GGGGS (Fig. 1). The protein was expressed in the insoluble fraction, and solubilized using 8 M urea. The refolding was carried out by stepwise dilution of urea, as described in the "Materials and Methods" section. Most of the scFv could be solubilized (95%) in the presence of 8 M urea, and only a little precipitation was observed during all the refolding steps. SDS-PAGE analyses for each purification step are shown in Fig. 2A, and the purity and yields are summarized in Table 1. Various refolding conditions were evaluated to increase the total amounts of correctly refolded scFv. The efficiency seems to be better when the sample concentration during dialysis is kept below 100 μM. The final step of purification using an antigen column indicates that ~1.5% of the solubilized protein is correctly refolded, possessing antigen binding ability. To analyze the oligomeric state of scFv, analytical ultracentrifugation experiments were carried out (Fig. 2B). The main peak (24.9 kDa, Fig. 2C) corresponded to the expected molecular mass (theoretical value, 27.1 kDa), indicating that the purified C6 scFv exists in a monomeric state (~96.6%).

The secondary structure of C6 scFv in the absence or presence of antigen was analyzed using CD spectroscopy (Fig. 3A). The results indicate that C6 scFv is folded and has a typical β-sheet rich structure. The far-UV CD spectrum remained unchanged upon antigen-binding. Thermodynamics of unfolding were analyzed using DSC (Figs. 3B and 3C). Thermal stability increased by ~18ºC upon the antigen binding (Table 2). Despite irreversible thermal unfolding, a two-state model was applied to fit the data, and thermodynamic parameters were determined (Table 2). The ratio of $\Delta H_{cal}/\Delta H_{vH}$ was approximately 1, indicating that C6 scFv transits to the unfolded state in cooperative manner.

The antigen binding ability of C6 scFv was analyzed using SPR biosensor (Fig. 4). In addition to the binding to immobilized NP-BSA, that to immobilized NNP-BSA was also analyzed, and the binding kinetics were determined (Table 3). The binding ability of C6 scFv is comparable to that of intact C6 reported previously [22]. Heterocliticity was observed since binding affinity to NNP was higher relative to NP. Taken together with the results of structural and physical analyses using CD and DSC, the antigen binding analyses indicate that C6 scFv is likely refolded correctly and has a functional structure.

The structural fluctuation of C6 scFv in the absence or presence of antigen was analyzed using DXT measurements. C6 scFv was immobilized on the Ni^{2+}-chelated substrate via its N terminal His-tag. Gold-nanocrystals were labeled on the surface of scFv as a motion tracer. In order to label gold-nanocrystal at the specific site, N54M mutant of C6 scFv was used, because of tight interaction between gold and sulfate. The residue at VH54 locates in the CDR-H2 loop, making it possible to detect the effect of antigen binding on the structural dynamics. The crystal structure of germline-type of C6, N1G9, in complex with NP indicates that 54^{th} residue of heavy chain is exposed to the solvent with little effects on antigen binding [26]. The CD and SPR experiments showed that the N54M mutation has little effects on the secondary structure and antigen binding ability (data not shown). The motions of N54M C6 scFv in the absence or presence of NP were analyzed in two rotational directions, representing tilting (θ) and twisting (χ). More than 300 trajectories were tracked in each condition, and these traced data were used to get mean square angular displacement (MSD) curves (Fig. 5). In MSD analysis, the slopes of the curves for scFv were decreased upon the addition of NP either in θ or χ direction. The angular diffusion coefficients (D) calculated from the slope of the MSD curves are summarized in Table 4. The results indicate that the large-scale motions of scFv are suppressed upon the antigen binding.

Discussion

Based on previous reports [27,28], we carried out stepwise dialysis under different conditions to increase the refolding efficiency of our scFv. The purification step using an antigen column indicated that ~1.5% of the solubilized scFv could be refolded, while retaining antigen binding ability. The rest of the molecules were likely misfolded, and thus could not bind to the antigen. Although most of the scFv could be solubilized during the stepwise dialysis, even in the final 0 M urea step, the correctly refolded scFv was limited, which can be detected by using antigen column. The SDS-PAGE analysis performed under non-reducing conditions showed several bands corresponding not only to monomer but also to oligomers (data not shown), suggesting that incorrect disulfide bonding patterns are one of the reasons for misfolding. The antigen binding kinetic parameters of C6 scFv purified in this study are comparable to those of intact C6 antibody reported previously [21]. In the case of intact antibody, because of its two combining sites, avidity arising from multivalent binding is observed for the antigen immobilized sensor chip. In contrast, only monovalent binding is observed in the case of scFv, as expected. Anti-NP antibodies are known to bind to hapten analogs such as NNP with higher affinity than to the autologous hapten, which is referred to as heterocliticity [22]. This phenomenon was also observed for C6 scFv (Table 3), supporting the notion that C6 has a functional structure. The complex with NNP is more stable than that with NP, because of the additional van der Waals contacts with the nitro group of NNP [22]. This would result in a slower dissociation rate (Table 2). Taken together with the structural analyses using CD and ultracentrifugation (Figs. 2C and 3A), the results demonstrate that C6 scFv likely folds correctly and that it possesses antigen binding ability comparable to that of the Fv region from intact C6 antibody.

Thermal stability of C6 scFv was increased upon antigen binding (Table 2). To analyze the thermodynamic origin of the stability difference, the thermodynamic

parameters at 48.5ºC, the denaturation temperature in the absence of NP, were calculated using the ΔC_p value [29]. The results indicate that the increased stability upon antigen binding is mainly due to enthalpic contribution (Table 5). Intermolecular interactions between C6 scFv and NP would increase the enthalpy change. Upon antigen binding, the scFv structure itself is expected to become more rigid [14]. The rigid structure in the native state would contribute to the favorable enthalpy change associated with unfolding, partially compensated by the unfavorable entropy change. The other favorable contributions such as hydration would result in the entropy change for C6 scFv with NP same as that without NP (Table 5).

The DXT experiments could detect the structural dynamics of proteins at the single-molecule level. The coverage of scFv molecules on the gold surface could be analogized by the previous study on quartz crystal microbalance (QCM) using the same chemical reagents for immobilized His-tagged protein on the gold surface [30]. The QCM study showed that the coverage of His-tagged proteins on the gold substrate was 1.9 pmol/cm^2, corresponding to 1.1 molecules per 10 nm squares. Considering the diameter of gold-nanocrystal used for DXT study (several tens of nm) and its labeling efficiency for scFv, most of our DXT study would provide single molecule level information. As shown in Fig. 5, the slopes of the MSD curves were distinctly different between antigen free and bound forms in each direction. In the previous experiments using anti-NP Fab fragments, Fab molecules were immobilized on the substrate via amine-coupling [17]. Since anti-NP Fab fragments have ~20 Lys residues on their surface, the orientations of Fabs were heterogeneous. In this study, C6 scFv was immobilized via an N-terminal His-tag. Therefore, the scFv molecules could be immobilized uniformly, and bind to antigens in a fashion similar to those in solution. In this study, we chose the residue at VH54 (Met) to label with gold nanocrystals, because it is exposed to solvent and is located at CDR2, whose movements would be greatly affected by antigen binding. MSD analysis showed that the movements of scFv

molecules in both θ and χ directions appeared suppressed upon addition of NP (Fig. 5). The functional and specific motions for χ angle were observed in some cases [18,19]. The DXT experiments using C6 Fab also produced the decreased slopes in MSD curves upon the antigen binding, especially in θ direction. The angular motion can be converted to translational length (*d*) by assuming a center axis for rotation using the equation, $d = r\alpha$, where *r* is the radius of rotation and α is the angle rotation in radians. The MSD values from Fabs ranged from about 1 to 3 $Å^2$ at a few hundred msec [17]. In the present study using C6 scFv, the value was within 10 mrad at a few hundred μsec. When this value is converted into $Å^2$ units at msec scale (assuming the *r* value of scFv is 50 Å), the MSD from scFv is ~2 $Å^2$, comparable to the Fab results.

As described previously [17], antigen binding energy could be calculated from the *D* values, using the following equation,

$$\Delta G = -RT \ln K_a = \alpha \ln(D_b/D_f) + \beta$$

where D_f and D_b are the values for antigen free and bound states, respectively. Using the values of α (14.6 kJ/mol) and β (–30.1 kJ/mol) determined previously [17], Δ*G* values are estimated to –41.5 and –43.5 kJ/mol for θ and χ angles, respectively. These values are in good agreement with that determined in the present SPR experiments, –46.9 kJ/mol (Table 3), suggesting that the fluctuations detected at the single-molecule level are well reflected from the antigen binding event in solution.

Using refolded scFv, it is possible to analyze how the structural dynamics change upon antigen binding. It will be interesting to compare the results of our DXT experiments with those from other biophysical methods such as NMR and calorimetry, which provide structural "ensemble" information. Additionally, in comparison with other scFv molecules derived from anti-NP antibodies on the pathway of affinity maturation, we can determine the correlation of structural dynamics with evolution, and apply the molecular basis for rational protein design [31,32]. We anticipate that systematic analysis of the structural dynamics of antibodies during affinity maturation

will greatly contribute to our understanding of structure-function relationships in proteins. Ongoing efforts in our group are attempting to generate other scFv molecules, derived from the anti-NP antibodies obtained at the different stage of affinity maturation, and analyze their differences from C6 scFv in structural and physical properties.

Acknowledgements

The synchrotron radiation experiments were performed at the BL40XU of SPring-8 with the approval of the Japan Synchrotron Radiation Research Institute (JASRI) (Proposal No. 2014A1153, 2013A1171, 2013A1883, and 2012B1199). The SPR experiments were performed at the Kyoto Integrated Science & Technology Bio-Analysis Center (KIST-BIC).

References

[1] H.N. Eisen, G.W. Siskind, Biochemistry 3 (1964) 996-1008.

[2] C. Milstein, C. Rada, Immunoglobulin Genes, second edition, Academic Press (1995) 57-81.

[3] T. Azuma, Immunol. Rev. 162 (1998) 97-105.

[4] G.J. Wedemayer, P.A. Patten, L.H. Wang, P.G. Schultz, R.C. Stevens, Science 276 (1997) 1665-1669.

[5] J. Yin, E.C. Mundorff, P.L. Yang, K.U. Wendt, D. Hanway, R.C. Stevens, P.G. Schultz, Biochemistry 40 (2001) 10764-10773.

[6] R. Adhikary, W. Yu, M. Oda, R.C.Walker, T. Chen, R.L. Stanfield, I.A. Wilson, J. Zimmermann, F.E. Romesberg, Biochemistry 54 (2015) 2085-2093.

[7] J. Foote, C. Milstein, Proc. Natl. Acad. Sci. U. S. A 91 (1994) 10370-10374.

[8] M. Oda, A. Kitai, A. Murakami, M. Nishimura, T. Ohkuri, Y. Abe, T. Ueda, H. Nakamura, T. Azuma, Arch. Biochem. Biophys. 494 (2010) 145-150.

[9] Y.O. Kamatari, S. Ohta, Y. Inoshima, M. Oda, M. Maruno, Y. Kobayashi, N. Ishiguro, Protein Sci. 23 (2014) 1050-1059.

[10] I.C. Wilkinson, C.J. Hall, V. Veverka, J.Y. Shi, F.W. Muskett, P.E. Stephens, R.J. Taylor, A.J. Henry, M.D. Carr, M.D. J. Biol. Chem. 284 (2009) 31928-1935.

[11] M. Acchione, Y.C. Lee, M.E. DeSantis, C.A. Lipschultz, A. Wlodawer, M. Li, A. Shanmuganathan, R.L. Walter, S. Smith-Gill, J.J.Jr Barchi, Biochemistry 51 (2012) 6017-6027.

[12] M. Taketani, A. Naitoh, N. Motoyama, T. Azuma, Mol. Immunol. 32 (1995) 983-990.

[13] K. Furukawa, A. Akasako-Furukawa, H. Shirai, H. Nakamura, T. Azuma, Immunity 11 (1999) 329-338.

[14] T. Sagawa, M. Oda, M. Ishimura, K. Furukawa, T. Azuma, Mol. Immunol. 39 (2003) 801-808.

[15] A. Murakami, Y. Takahashi, M. Nishimura, T. Shimizu, T. Azuma, Mol. Immunol. 48 (2010) 48-58.

[16] Y.C. Sasaki, Y. Suzuki, N. Yagi, S. Adachi, M. Ishibashi, H. Suda, K. Toyota, M. Yanagihara, Phys. Rev. E Stat. Phys. Plasmas. Fluids Relat. Interdiscip. Topics 62 (2000) 3843-3847.

[17] T. Sagawa, T. Azuma, Y.C. Sasaki, Biochem. Biophys. Res. Commun. 355 (2007) 770-775.

[18] H. Shimizu, M. Iwamoto, T. Konno, A. Nihei, Y.C. Sasaki, S. Oiki, Cell 132 (2008) 67-78.

[19] H. Sekiguchi, A. Nakagawa, K. Moriya, K. Makabe, K. Ichiyanagi, S. Nozawa, T. Sato, S. Adachi, K. Kuwajima, M. Yohda, Y.C. Sasaki, PloS one 8 (2013) e64176.

[20] H. Sekiguchi, Y. Suzuki, Y. Nishino, S. Kobayashi, Y. Shimoyama, W. Cai, K. Nagata, M. Okada, K. Ichiyanagi, N. Ohta, N. Yagi, A. Miyazawa, T. Kubo, Y.C. Sasaki, Sci. Rep. 4 (2014) 6384.

[21] M. Oda, T. Azuma, Mol. Immunol. 37 (2000) 1111-1122.

[22] M. Oda, T. Azuma, Mol. Immunol. 70 (2016) 8-12.

[23] P. Schuck, Biophys. J. 78 (2000) 1606-1619.

[24] S. Inaba, H. Fukada, M. Oda, Int. J. Biol. Macromol. 82 (2016) 725-732.

[25] Y. Okumura, T. Miyazaki, Y. Taniguchi, Y.C. Sasaki, Thin Solid Films 471 (2005) 91-95.

[26] R. Mizutani, K. Miura, T. Nakayama, I. Shimada, Y. Arata, Y. Satow, J. Mol. Biol. 254 (1996) 208-222.

[27] K. Tsumoto, K. Shinoki, H. Kondo, M. Uchikawa, T. Juji, I. Kumagai, J. Immunol. Methods 219 (1998) 119-129.

[28] M. Umetsu, K. Tsumoto, M. Hara, K. Ashish, S. Goda, T. Adschiri I. Kumagai, J. Biol. Chem. 278 (2003) 8979-8987.

[29] S. Inaba, H. Fukada, T. Ikegami, M. Oda, Arch. Biochem. Biophys. 537 (2013) 225-232.

[30] A. Thammasittiron, M. Dechklar, S. Leetachewa, K. Pootanakit, C. Angsuthanasombat, Appl. Environ. Microbiol. 77 (2011) 6836-6840.

[31] D. Lingwood, P.M. McTamney, H.M. Yassine, J.R. Whittle, X. Guo, J.C. Boyington, C.J. Wei, G.J. Nabel, Nature 489 (2012) 566-570.

[32] J.G. Jardine, T. Ota, D. Sok, M. Pauthner, D.W. Kulp, O. Kalyuzhniy, P.D. Skog, T.C. Thinnes, D. Bhullar, B. Briney, S. Menis, M. Jones, M. Kubitz, S. Spencer, Y. Adachi, D.R. Burton, W.R. Schief, D. Nemazee, Science 349 (2015) 156-161.

Figure Legends

Fig. 1. Design of C6 scFv. Fv domains of anti-NP antibody N1G9 (PDB code, 1NGP) are shown schematically as an scFv. C terminus of VL (gray) and N terminus of VH (black) domains were connected with a $(G_4S)_3$ linker (broken line).

Fig. 2. SDS-PAGE and ultracentrifugation analyses. (A) 15% SDS-PAGE gel showing fractions from each purification step; lane 1: after sonication, 2: soluble fraction; supernatant of sonicated suspension, 3: solubilization of insoluble fraction, 4: collected fraction after stepwise dialysis, 5: after thrombin digestion to remove fused tag at N terminus, 6: eluate of antigen column using 10 mM Gly-HCl (pH 2.7), 7: protein molecular weight marker. (B) Sedimentation pattern and best fit result obtained from the c(s) analysis of a solution of C6 scFv. Residuals between observed data and best-fit result are also indicated. (C) Distribution of C6 scFv.

Fig. 3. Secondary structure and thermal stability analyses. (A) Far-UV CD spectra of C6 scFv in the absence (solid line) or presence (broken line) of NP-Cap. In DSC analysis of C6 scFv, heat capacity curves (solid lines) were monitored without antigen (B) and in the complex with NP at a molar ratio of 1:10 (C). Baselines (dotted lines) were determined by fitting analysis.

Fig. 4. Antigen binding analysis. $NP_{8.2}$-BSA (A) and $NNP_{6.4}$-BSA (B) were immobilized on a CM5 sensorchip and the scFv (0.781, 1.56, 3.13, 6.25, 12.5, 25.0, 50.0, 100, 200, 400, and 800 nM) was flowed over the chip surface at rate of 20 μl/min for 3 min, followed by 3 min dissociation.

Fig. 5. MSD curves for θ and χ directions. C6 scFv was immobilized on the Ni^{2+}-chelated substrate and Laue spots were monitored from gold-nanocrystals attached to the scFv molecules. The motions of C6 were traced, both in free form (open circle) and in complex with antigen (closed circle).

Table 1. Purification of C6 scFv.

	total proteins (mg)	C6 scFv (mg)	purity (%)	yield (%)
culture (500 mL)	545	80 [a]	14.6	100
soluble fraction	425	0	–	0
solubilization	147	76 [a]	52	95
antigen column	1.2	1.2	> 90	1.5

These values were estimated from the bands on SDS-PAGE gel using ImageJ, open source image processing program.

[a] The values correspond to the mass of C6 scFv without N-terminal thioredoxin-tag.

Table 2 Thermodynamic parameters for denaturation of C6 scFv in the absence or presence of NP analyzed using DSC.

	T_d (°C)	ΔH_{cal} (kJ/mol)	ΔH_{vH} (kJ/mol)	$\Delta H_{cal}/\Delta H_{vH}$	ΔC_p (kJ/mol·K)
C6 scFv	48.5 ± 0.03	370 ± 1	355	1.04	7.46 ± 0.73
C6 scFv + NP	66.7 ± 0.03	511 ± 7	474	1.07	6.95 ± 1.66

The S.D. derived from fitting is given.

Table 3 Kinetic parameters of interactions of C6 scFv to hapten-BSA conjugates.

	k_{on} ($\times 10^6$ M^{-1} s^{-1}) [a]	k_{off} ($\times 10^{-3}$ s^{-1}) [a]	K_a ($\times 10^8$ M^{-1}) [b]
NP-BSA	1.28 ± 0.20	7.81 ± 0.62	1.64
NNP-BSA	1.32 ± 0.24	1.99 ± 0.23	6.63

The S.E. derived from three measurements is given.

[a] The k_{on} and k_{off} are the average of three experiments for protein concentrations from 0.78 to 800 nM.

[b] The K_a are calculated from the two rate constants: $K_a = k_{on}/ k_{off}$.

Table 4 Angular diffusion coefficient of C6 scFv in the θ and χ directions.

	Angular Diffusion coefficient: D (rad²/sec)
C6 antigen free (θ)	2.04 (± 0.03) × 10^{-5}
C6 + NP (θ)	9.34 (± 0.07) × 10^{-6}
C6 antigen free (χ)	8.65 (± 0.12) × 10^{-6}
C6 + NP (χ)	3.46 (± 0.09) × 10^{-6}

The values were obtained from the slope (Angular diffusion coefficient: *D*) of the MSD curves (Fig. 5). *D* values were calculated with following equation: $MSD = 4Dt + A$, where *MSD* is the mean square displacement, *t* is time interval and A is the intercept of the fitting line. The S.D. derived from fitting is given.

Table 5 Thermodynamic parameters for denaturation of C6 scFv at the denaturation temperature in the absence of NP (48.5ºC).

	T_d [a] (ºC)	ΔG (kJ/mol)	ΔH (kJ/mol)	(kJ/mol)	$T\Delta S$ [b]
C6 scFv	48.5	0	370		370
C6 scFv + NP	66.7	24	394		370

[a] The T_d values were taken from Table 2.

[b] $T\Delta S$ values were calculated from the equation, $\Delta G(T) = \Delta H(T) - T\Delta S(T)$.

Fig. 1

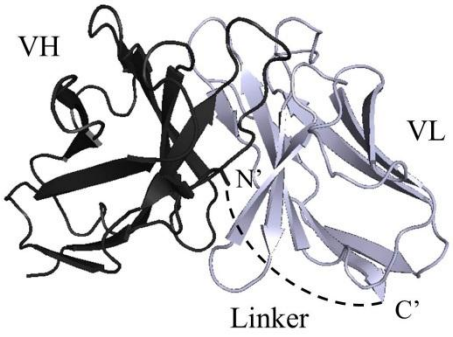

Fig. 2

(A)

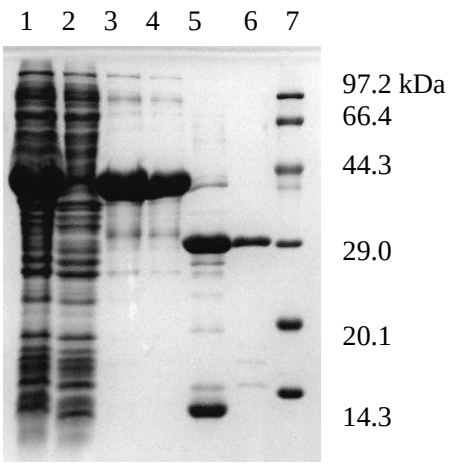

(B)

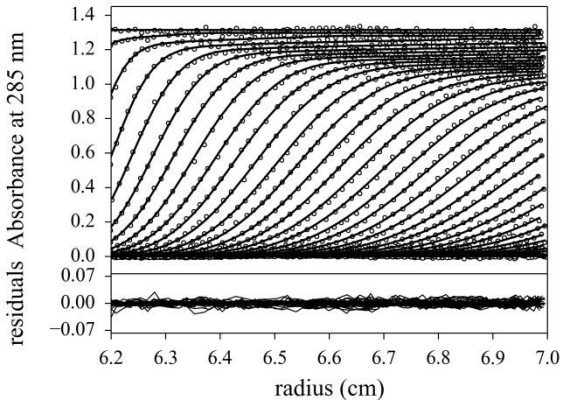

(C)

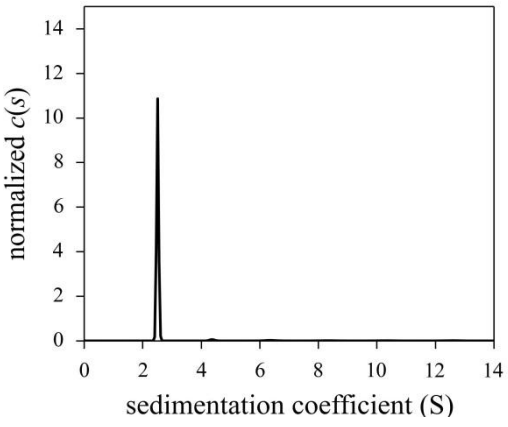

Fig. 3

(A)

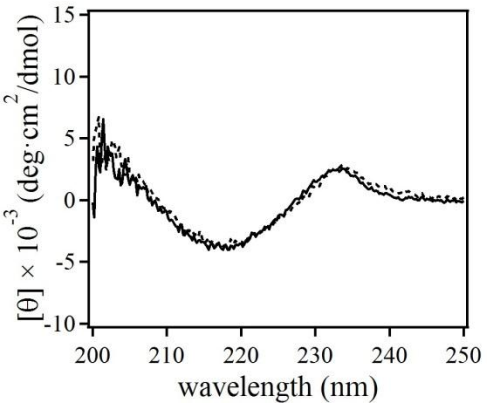

(B)

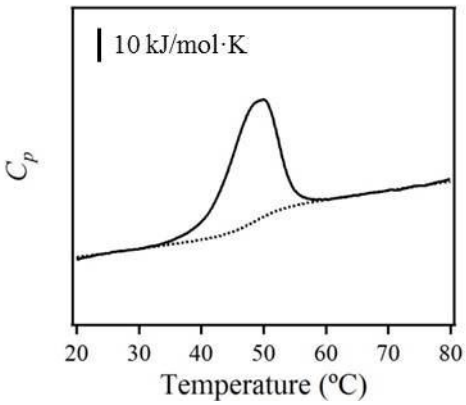

(C)

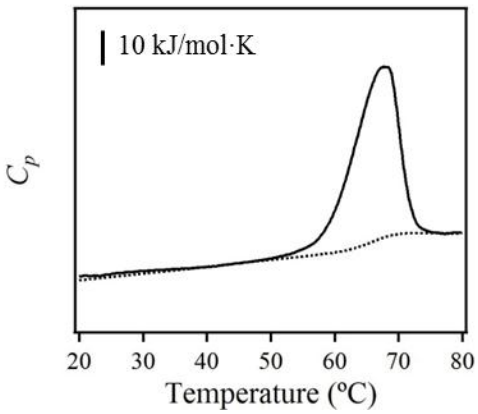

Fig. 4

(A)

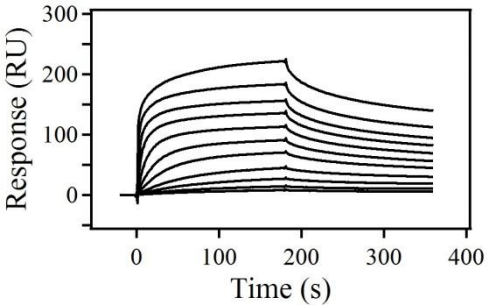

(B)

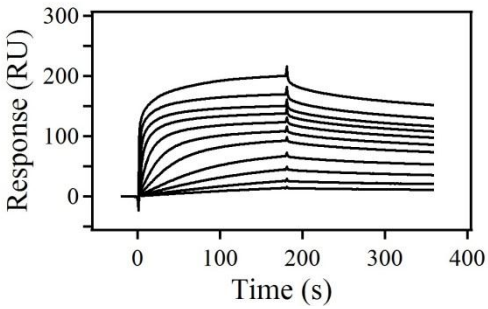

Fig. 5